Effects of sensory precision on mobile robot localization and mapping

J.G. Rogers III, A.J.B. Trevor, C. Nieto-Granda, A. Cunningham, M. Paluri, N. Michael, F. Dellaert, H.I. Christensen, V. Kumar

Abstract This paper will explore the relationship between sensory accuracy and Simultaneous Localization and Mapping (SLAM) performance. As inexpensive robots are developed with commodity components, the relationship between performance level and accuracy will need to be determined. Experiments are presented in this paper which compare various aspects of sensor performance such as maximum range, noise, angular precision, and viewable angle. In addition, mapping results from three popular laser scanners (Hokuyo's URG and UTM30, as well as SICK's LMS291) are compared.

1 Introduction

Robots are ideally suited for exploration tasks in dangerous environments such as a disaster site or urban counter-insurgency operations. Simultaneous Localization and Mapping (SLAM) techniques can be used to build maps which can be shared with emergency workers or soldiers as the robots complete their exploration mission [5]. Projects such as the Micro Autonomous System Technologies Collaborative Technology Alliance (MAST CTA) [1] are working to develop techniques and components to enable robot mapping with low power and small form factor robots and sensors. MAST's mission is to develop robots which are autonomous and collaborate to provide situational awareness in urban environments for military and rescue operations. MAST platforms are required to have a small form factor and long operational availability, so we must understand where compromises can be made on sensor performance.

J. Rogers, A. Trevor, C. Nieto-Granda, A. Cunningham, M. Paluri, F. Dellaert, H. Christensen
Georgia Institute of Technology,e-mail: {jgrogers, atrevor, carlos.nieto, alexgc, balamanohar, dellaertf, hic}@ gatech.edu

N. Michael, V. Kumar
University of Pennsylvania, e-mail: nmichael@seas.upenn.edu, kumar@grasp.upenn.edu

There is a need to determine what level of performance is needed from sensors to enable SLAM techniques to deliver a map of sufficient quality after autonomous exploration of an unknown environment. Sensors such as laser scanners are available in laboratory applications but other sensory modalities such as radar or vision may be preferred when considering cost levels, power usage, and size. Some of the accuracy, density, annular confinement, and field of view assumptions which are common with laser scanners might no longer be valid with these other sensory modalities. Low cost radar based scanners are currently under development as part of the MAST project; until these are available, we will simulate the performance of radar in software using data from laser scanners. To investigate the effects of various properties of a sensor on the mapping result, we use high quality laser data and degrade properties such as the maximum range, angular resolution, field-of-view, or range accuracy. We call this *de-featuring* the data. The performance requirements for robot mapping must be determined to guide the development of these new miniaturized radar scanners to ensure that they will work well for the robot mapping task.

A comparison of related works is presented in section 2. The technical details of our algorithms are presented in section 3. The experimental procedure is presented in section 5 and results are analyzed in section 6. Some of the more interesting results are explored in section 7.

2 Related Works

The Extended Kalman Filter (EKF) was first used for mobile robot localization in [7] and [8] with an *a priori* map. These techniques were extended by Smith *et.al.* in [20] by including the landmark positions in the state vector to produce one of the first viable solutions to the SLAM problem. A thorough review of the early approaches to the SLAM problem can be found in the summary paper by Durrant-Whyte and Bailey [11]. Their second summary paper gives an overview of the state-of-the-art approaches to the SLAM problem [4].

The computer vision community has developed Structure from Motion (SFM) techniques to solve an analogous problem to SLAM. These techniques maintain the entire robot trajectory instead of marginalizing out all but the last pose; some techniques such as bundle adjustment solve for all relevant parameters simultaneously [2]. Landmarks and poses remain uncorrelated by not marginalizing out the robot trajectory, and can therefore be represented without forming an n^2 covariance matrix. This can result in a significantly more efficient algorithm. Solving for the entire robot trajectory along with the map is called the *full SLAM* problem.

Nonlinear optimization techniques were used by Folkesson and Christensen in [12] to close loops without linearization errors. Dellaert introduced Square Root Smoothing and Mapping (SAM) which uses a sparse matrix representation to efficiently solve for landmark locations and the robot trajectory in [9] and [10]. An incremental version of this technique was further deveoped in [15] and [16] which

use QR factorization and periodic reordering of the underlying matrix representation to maintain real-time performance.

An objective benchmark for comparing SLAM algorithms was reported in [6]. This benchmark compares the incremental relative error along the robot's trajectory instead of comparing maps. This allows the authors to directly compare the results between different algorithms or sensor types. Ground truth is generated by manually aligning laser scans using ICP as an initial guess. We use the relative pose error metric and ground truth generation method from this benchmarking paper to asses SLAM performance levels under various sensor configurations.

Research has been reported on analysis of localization performance and sensing characteristics. O'Kane and Lavalle proved that it is possible to localize in a known map with a robot equipped with only a contact sensor and a compass in [19] and [14]. The authors determined that it is impossible to localize a robot in a known map if the compass is replaced with an angular odometer. In the SLAM domain, work has been done to support simpler and less expensive sensor modalities. Bailey developed techniques for delaying initialization of landmarks in bearing-only SLAM in [3]. A paper by Müller *et.al.* relates the performance of their 6D SLAM algorithm to the precision of their 3D laser scanner in [17].

3 Technical Approach

The mapper used in this paper is based upon the Georgia Tech Smoothing and Mapping (GTSAM) library. The GTSAM library optimizes a nonlinear *factor graph* of robot measurements to recover the trajectory and map. This representation preserves sparsity by maintaining the trajectory as well as the landmark positions within the state vector. The GTsam library is based upon Dellaert's *Square Root SAM* technique [9]. The nonlinear factor graph is composed of odometry factors between subsequent poses and measurement factors between wall landmarks and poses. To make a nonlinear factor, we need an error function and its derivatives. The implementation for the odometry factor is provided by the GTSAM library through generic programming for all objects which belong to a *Lie group*.

The nonlinear factor for wall landmark measurements relates the position of the wall to the robot. Frequently, we cannot make a measurement of the entire length of a wall from a single position due to limited range and environmental occlusion. We have augmented GTSAM's nonlinear factor representation with the M-space feature representation [13] to allow for partial observation and to leverage multiple types of landmarks for different applications.

The M-space feature representation is useful for expressing measurements of partially observed objects, such as walls seen with limited range or with environmental occlusion. The M-space representation effectively corrects based upon the infinite line representation in this implementation. It is possible to upgrade this representation to include the endpoints as they are fully observed; however, this is reserved for future work. Currently, the measurement correction corresponds to the angle

and range to the wall, $\eta = (\phi, \rho)$. Endpoints, along with angle and range, are used for data association. The factor graph representation requires the Jacobians of these measurements which are $\frac{\delta \eta}{\delta x_r}$ and $\frac{\delta \eta}{\delta x_f}$ where x_r is the robot pose and x_f is the global landmark pose. The M-space feature representation uses the chain rule to represent Jacobians in terms of smaller building blocks which are re-usable between different types of features.

In the M-space feature representation, the Jacobians are broken down in terms of local parameterizations of the landmarks (x_o) to $\frac{\delta \eta}{\delta x_r} = \frac{\delta \eta}{\delta x_o} \frac{\delta x_o}{\delta x_r}$. The transformation from the local reference frame x_o to the global frame x_f is a simple rigid body transformation. The Jacobian of this transformation is the derivative of these local representation x_o with respect to the robot pose x_r which is $\frac{\delta x_o}{\delta x_r} = \begin{bmatrix} -1 & 0 & x_{o_y} \\ 0 & -1 & -x_{o_x} \end{bmatrix}$

For completeness, the Jacobian $J_{\eta o}$ for walls is provided here. Let $\left(x^1_{o_x}, x^1_{o_y}, x^2_{o_x}, x^2_{o_y}\right)$ be the coordinates of the endpoints of the walls. Let dy be the y-coordinate difference in the endpoints of the wall $x^2_{o_y} - x^1_{o_y}$, and let dx be the x coordinate difference $x^2_{o_x} - x^1_{o_x}$. Also, let L be the length of the wall, $L = \sqrt{dx^2 + dy^2}$.

$$J^T_{\eta o} = \frac{\delta \eta^T}{\delta x_o} = \begin{bmatrix} \frac{-dy}{L^2} & \frac{-dy*\left(dx*x^2_{o_x} + dy*x^2_{o_y}\right)}{L^3} \\ \frac{dx}{L^2} & \frac{dx*\left(dx*x^2_{o_x} + dy*x^2_{o_y}\right)}{L^3} \\ \frac{dy}{L^2} & \frac{dy*\left(dx*x^1_{o_x} + dy*x^1_{o_y}\right)}{L^3} \\ \frac{-dx}{L^2} & \frac{-dx*\left(dx*x^1_{o_x} + dy*x^1_{o_y}\right)}{L^3} \end{bmatrix} \tag{1}$$

Equation 1 is the Jacobian relating the error from the robot relative position with respect to the landmark.

$$\frac{\delta \eta}{\delta x_f} = \frac{\delta \eta}{\delta x_o} \frac{\delta x_o}{\delta x_f} \tilde{B} \tag{2}$$

Equation 2 shows the overall Jacobian relating error from the global representation with respect to the landmark. In this equation, $\tilde{B}$ is the binding matrix which projects corrections from the M-space representation (ϕ, ρ) to the endpoint representation x_f. In this way, the corrections will only be applied to the direction and distance of the line, but not to the endpoints themselves. The M-space source paper [13] should be consulted for more implementation details.

The feature detectors developed for this mapping application have been designed to be robust to noise and performance degradation. We have chosen to extract line segments from laser range data using a RANSAC technique described in [18]. First, points which are at maximum range are eliminated from the scan. Pairs of points are then chosen uniformly from the laser scan and a line hypothesis is made which passes through these points. If enough other points are consistent with this line hypothesis, then the inliers to the line hypothesis are used to form a more accurate hypothesis. The inlier points are then removed from the laser scan so that each line will be unique. This process is repeated for a number of iterations to ensure that we

extract many of the lines in the scene. We have selected parameters such as minimum line length and maximum gap which correspond to the size of walls and door openings in a typical office environment.

The experiments in this paper were run on data collected from two types of mobile robots and were processed offline to compare mapping performance with different sensor accuracies. Though these techniques were compared in offline operation, it should be noted that the mapper can comfortably run online on a modest CPU.

4 Experimental Design

The operation of the experimental framework is shown in figure 1. Ground truth was generated by manual alignment of the full unaltered laser scan data in an initial run. This serves as an adequate estimate of ground truth for the purpose of this relative comparison of path trajectory error with different sensor performance levels. The manual alignment tool can be seen in figure 2. It allows the operator to correct the (x, y, θ) between two poses so that the laser scans come into alignment. This information is then captured in a ground-truth file where it is compared to the posterior relative displacements in the test run trajectories.

Stored robot data is replayed with various settings of laser scan data de-featuring. The laser line extractor extracts line segments from the de-featured laser data and sends it to the mapper. Once the run is complete, the robot trajectory from the mapper is compared to the ground truth for this run. The average incremental absolute error is then recorded for this run.

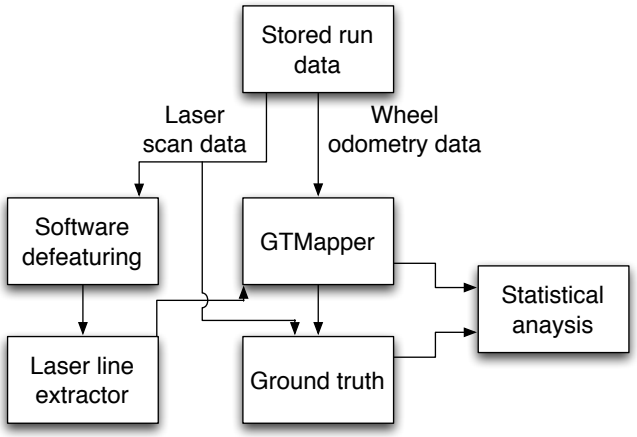

Fig. 1 The experimental setup.

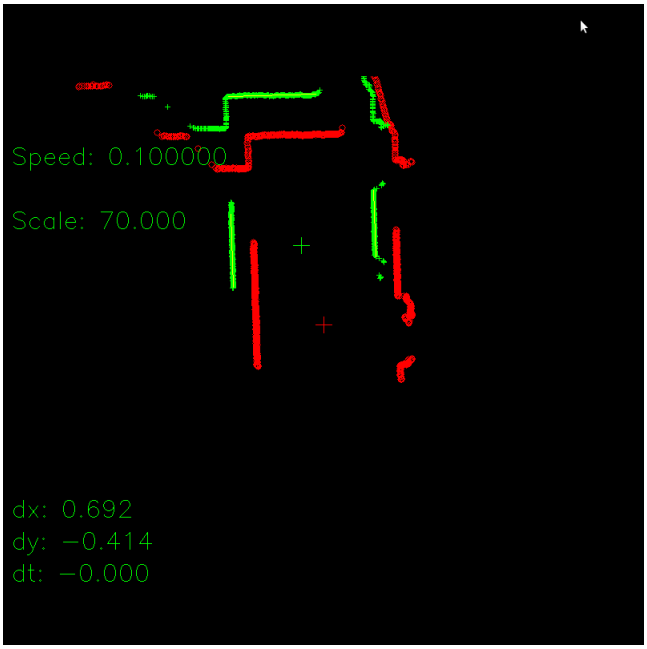

Fig. 2 The alignment tool used to generate ground truth trajectories. Poses illustrated in this figure are displayed at a poor solution to illustrate operation.

5 Experiments

The first source of sensor data used in these experiments was a series of logs taken from the *Scarab* robots developed at the University of Pennsylvania. An image of the Scarab robot can be seen in figure 3. The Scarab is a differential drive mobile robot equipped with a Hokuyo URG laser scanner. In this series of experiments, the robot was tele-operated for ten runs in an indoor office environment to collect data which is used for offline processing.

The laser scanner accuracy was de-featured for our analysis to determine what level of performance in the mapping task can be expected with progressively simpler (and therefore less expensive and lower power) sensors. All sensor values were captured during the data collection phase and were de-featured with software in the post-processing phase.

In the first round of experiments, several de-featuring modifications were made to the laser scanner readings. First, the range of the scanner was restricted. Second, the angular precision of the laser scanner was limited by omitting beams from the line extraction process. Thirdly, the angle subtended by the laser scan was reduced. Finally, the range accuracy of the sensor was corrupted by varying degrees of Gaussian noise. This series of experiments will establish which parameters of the scanner can be varied while still yielding sufficient performance in the mapping task.

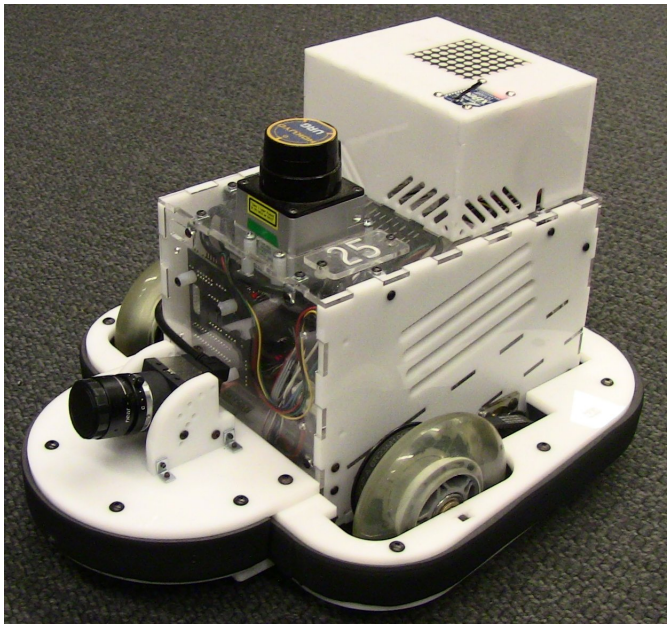

Fig. 3 The Scarab mobile robot developed at the University of Pennsylvania.

In the second experiment, the Georgia Tech robot "Jeeves" was outfitted with three different laser scanners to collect a run where each laser can be used to compare the mapping results. The robot is a Segway RMP 200 modified to be statically stable, as seen in figure 4. This platform is configured to simultaneously collect data from the SICK LMS291, Hokuyo URG, and the Hokuyo UTM 30 laser scanners, all of which are seen in the right of figure 4. This data is used individually in the mapping process and the resultant relative errors are compared. In this experiment, there is no need to de-feature the performance of the laser scanners in software since each exhibits a unique price and performance level.

6 Results

In the first set of experiments, Scarab robots were driven along a similar trajectory in an office building 10 times. Two of the runs were of poor quality due to wheel slip on a thick concrete seam and were eliminated from the analysis. In figure 5 the mean trajectory error is displayed from a series of test runs where the maximum range of the laser scanner was varied from 5.6 meters down to 0.4 meters. 5.6 meters is the maximum range of the Hokuyo URG laser scanner. It can be seen from this figure that the performance is poor when the range is restricted to below 2 meters, but it rapidly improves at longer ranges to a nearly constant level of performance. The

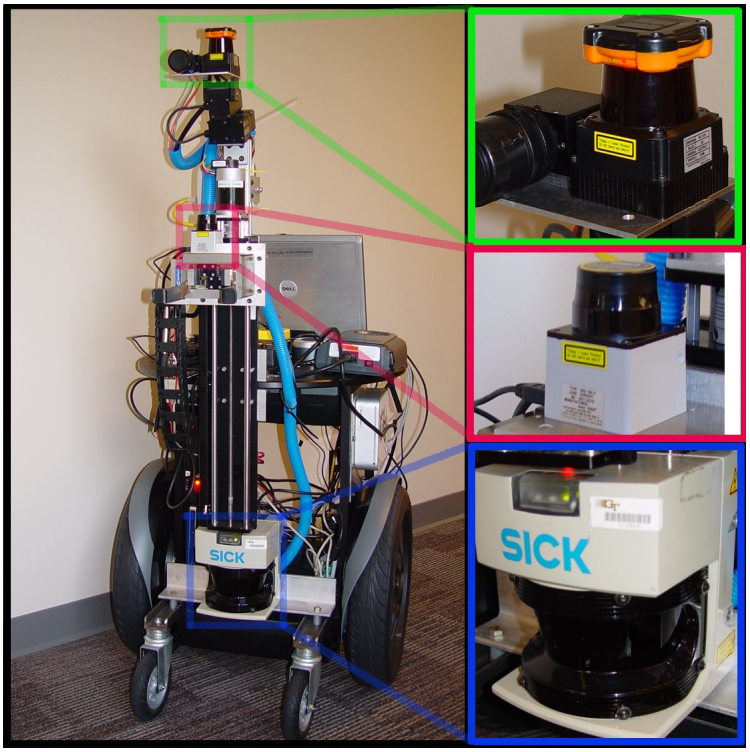

Fig. 4 The Georgia Tech robot "Jeeves". Left: Full robot platform. Right-top(green): Hokuyo UTM-30 laser scanner. 30 meter maximum range, 270 degree viewing angle, 0.25 degree angular resolution. Right-middle(magenta): Hokuyo URG laser scanner. 5.6 meter maximum range, 270 degree viewing angle, 1 degree angular resolution. Right-bottom(blue): SICK LMS291 laser scanner. 80 meter maximum range, 180 degree viewing angle, 1 degree angular resolution.

residual incremental error (due to the inaccuracy in the odometry of the robot) is reached as the range is restricted to 0.8m and below. This experiment indicates that the accuracy of the mapper can be maintained until the range of the laser scanner is restricted to about 1.6 meters, roughly the width of the hallways in the test site.

In figure 6 the mean trajectory error is displayed from a series of test runs where progressively higher proportions of the laser beams are left out of the line extraction process. This test is meant to simulate a sensor with less angular resolution than the Hokuyo URG. It is apparent from the graph that until the resolution is lowered to around 1 degree, the mapper is able to deliver a similar level of performance to the results from the fully featured laser scan. This corresponds to throwing away 75% of the data coming from the laser scanner. When the resolution is lowered below 1 degree, the accuracy drops to the level of the robot odometry alone.

In figure 7 the mean trajectory error is compared with various angles viewed by the laser scanner. The default Hokuyo URG laser scanner can view 270 degrees. This metric is meant to simulate a sensor which views a smaller angle. The viewing

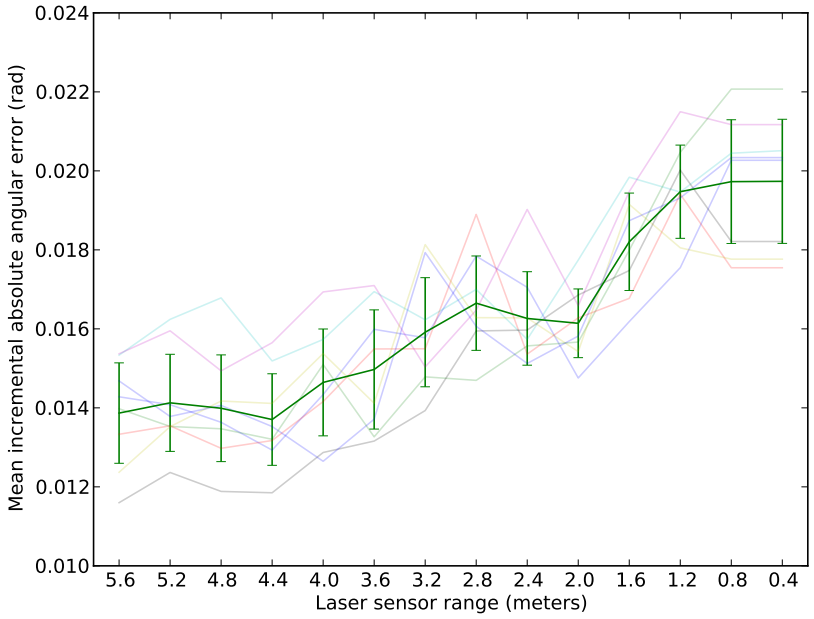

Fig. 5 Mean incremental heading error with various maximum range settings of laser scanner from 0.4m to 5.6m

angle is always faced towards the front as it is expected that the sensors would need to observe this region in order to avoid hitting obstacles during autonomous operation. This graph suggests that the mapper remains accurate until as little as 90 degrees is viewed from the laser scanner. This is probably due to the fact that in this test the range was kept at its maximum value of 5.6 meters, so the mapper was still able to see wall line segments. If the range was restricted while the angular view was also restricted, then we would expect poor performance.

In figure 8 the mean trajectory error is displayed from a series of test runs where Gaussian noise is added to the range measurements. The noise is sampled from a Gaussian distribution with the variance indicated along the x-axis. It can be seen from this figure that with even a moderate 2cm noise is added to the laser scan significant error is introduced into the map. The mapper is particularly susceptible to noise in the laser ranges, though it should be noted that this noise level is significantly higher than a typical laser scanner.s

In the second experiment, the mapping results were compared with three different laser scanners which are commonly used by the SLAM research community. An example map is show in figure 10. The robot successfully closed the loop with each of the laser scanners. The absolute relative incremental position and angular errors can be seen in table 9. It can be seen with these results that the SICK and URG map-

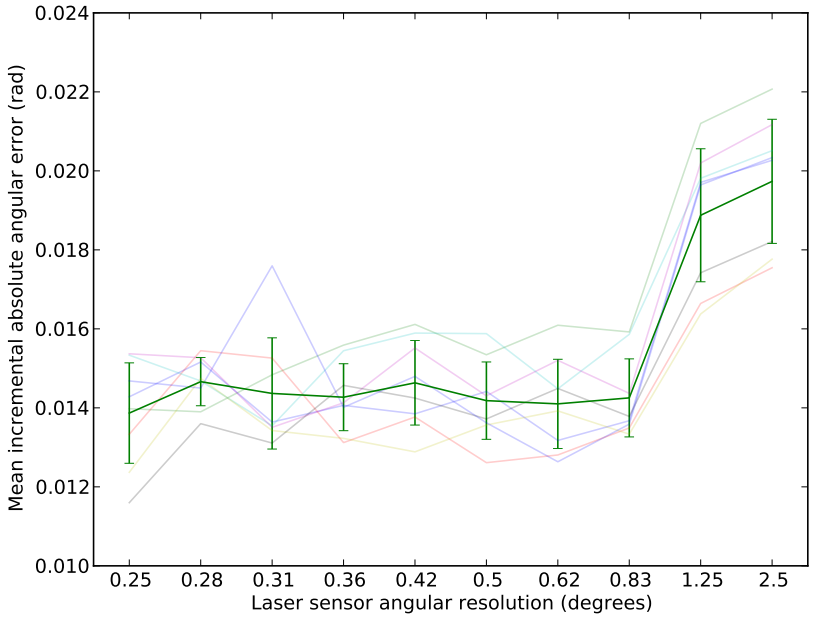

Fig. 6 Mean incremental heading error with various angular resolutions from 0.25 degrees to 2.5 degrees

ping results are pretty similar in displacement error, whereas the UTM30 is much more accurate in recovering the relative displacements. This is to be expected since the UTM30 slightly outperforms the SICK 291 laser scanner in angular resolution, range accuracy, and speed.

7 Discussion

The longer range of the laser scanner appears to not be helping much in the office environment. This indicates that the line extraction algorithm is working well when even a small amount of the wall can be seen from the scanner, so the range of the scanner doesn't need to be much more than the width of the hallway in order to achieve good performance. We believe that in general the range of the scanner needs to be no more than such that it can see about 1 meter of the wall from the middle of the hallway.

We were surprised to find that the mapper was so susceptible to range accuracy given that our line extraction algorithm performs a least-squares fit to many laser points and should be able to handle zero-mean noise. It should be noted that the

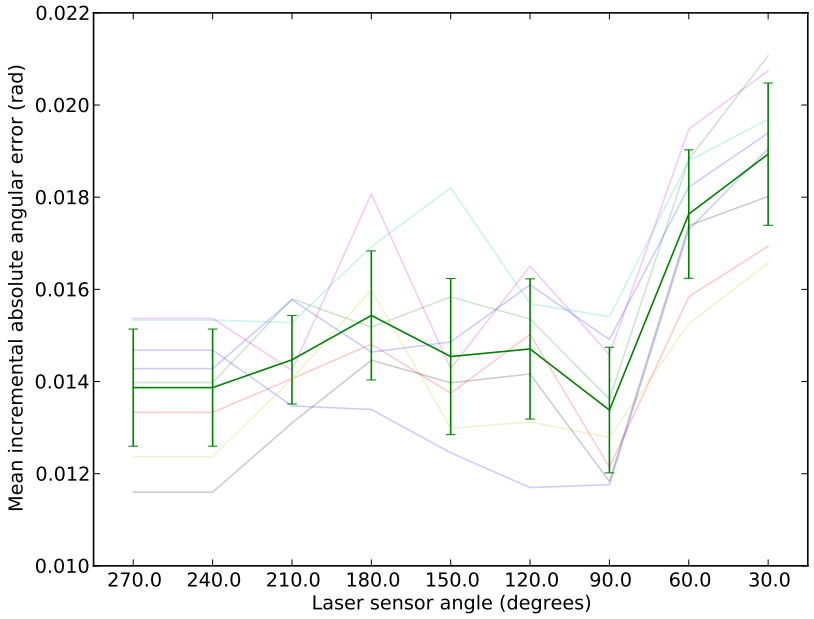

Fig. 7 Mean incremental heading error with various maximum laser angles

noise levels explored here were relatively large and that the line extraction performs very well for noise levels more typical of laser scanners. We believe that, with additional parameter tuning, the line extractor could be made to perform well with more noise; so this technique should translate well to radar scans.

The angular resolution parameter is effectively reducing the range of the scanner slightly because the missing resolution is causing gaps in the extracted lines beyond a certain range. This prevents long lines from being extracted; however, we have already determined that range much longer than the hallway width is not very important in the range test. We have now also determined that high angular resolution is not needed to perform the mapping task well.

For the second experiment with the robot "Jeeves", we notice that the incremental angular error is comparable between the SICK and UTM30 laser scanners, with the URG performing slightly worse. We believe this is because the office environment for the second experiment has larger, cluttered rooms for which the limited range would often result in few measurements of the walls with the URG. The incremental displacement error seems to show that the UTM30 is performing better than the SICK laser scanner. In our first experimental analysis we determined that the mapping results are particularly susceptible to range accuracy, but the The UTM30 claims a $\pm 30mm$ range accuracy whereas the SICK claims a $\pm 35mm$ range accuracy. There is only 5mm difference here so this is likely not the main cause. It is

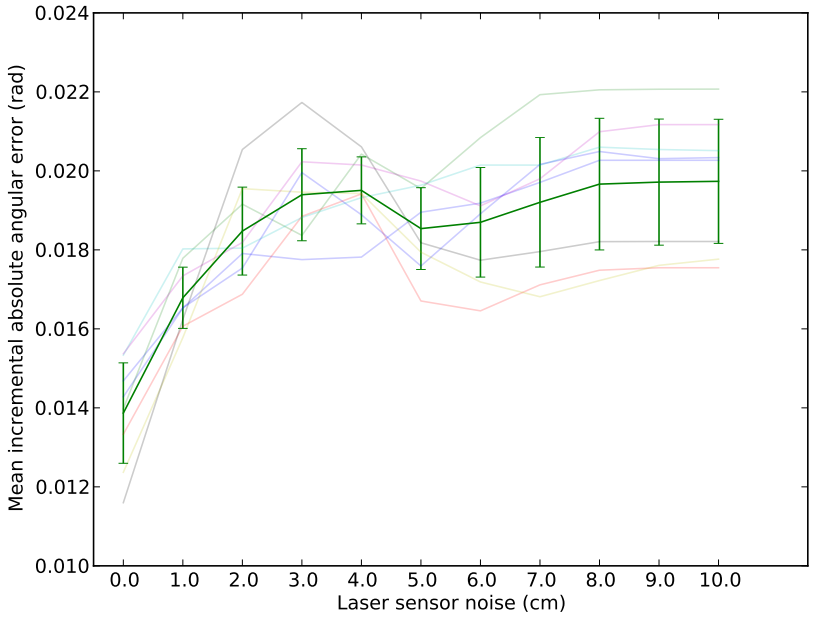

Fig. 8 Mean incremental heading error with various amounts of Gaussian noise added to laser ranges with variance up to 10cm

Error	URG	SICK	UTM-30
Position error	0.020162	0.020942	0.009785
Angular error	0.009924	0.006612	0.007033

Fig. 9 Absolute incremental position and orientation error for test comparing performance of mapping with three typical laboratory laser scanners

more likely that the extended viewing angle combined with the longer range of the UTM30 is allowing the robot to observe both the walls behind it as well as those in front of it for a significant portion of the run. The SICK can only see in front of the robot and is therefore only correcting based on the walls in front – it cannot see the wall behind the robot as it passes through a doorway. We think that this effect was not seen in the first experiment with the Scarab robots because they were operated in an environment with narrow corridors and few larger rooms. The Scarab robots never had the opportunity to pass through doorways and therefore could not benefit from this effect.

Based on these results, we determine that the Hokuyo UTM30 is the ideal laser scanner for use in environments with larger open spaces. It has additional advantages over the LMS291 laser scanner, namely size and power usage. In environments with more confined spaces, the Hokuyo URG performs well enough to make useful maps.

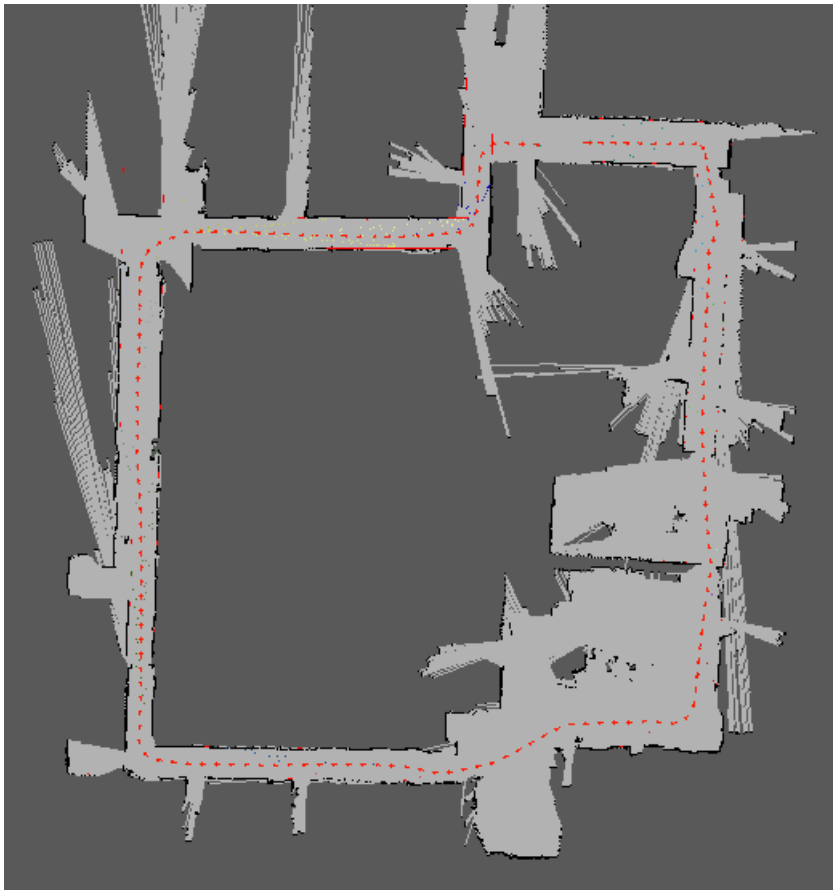

Fig. 10 The map of the the corridors in our lab. There are two large storage rooms in the lower right. The map is shown as an occupancy grid only for display purposes – all measurements are made based on wall features.

8 Acknowledgements

This work was made possible through the ARL MAST CTA project, the Boeing corporation, and the KORUS project.

References

[1] ARL (2006) MAST CTA. URL http://www.arl.army.mil/www/default.cfm?page=332
[2] B Triggs RIH PF McLauchlan, Fitzgibbon AW (1999) Bundle adjustment - a modern synthesis. Lecture Notes in Computer Science pp 298–372

[3] Bailey T (2003) Constrained initialisation for bearing-only SLAM. In: IEEE International Conference on Robotics and Automation
[4] Bailey T, Durrant-Whyte H (2006) Simultaneous localisation and mapping (SLAM): Part II state of the art. Robotics and Automation Magazine
[5] Berrabah SA, Baudoin Y, Sahli H (2010) SLAM for robotic assistance to fire-fighting services. In: World Congress on Intelligent Control and Automation
[6] Burgard W, Stachniss C, Grisetti G, Steder B (2009) Trajectory-based comparison of SLAM algorithms. In: In Proc. of the IEEE/RSJ Int. Conf. on Intelligent Robots & Systems (IROS)
[7] Chatila R, Laumond J (1985) Position referencing and consistent world modeling for mobile robots. International Conference on Robotics and Automation
[8] Crowley J (1989) World modeling and position estimation for a mobile robot using ultra-sonic ranging. International Conference on Robotics and Automation
[9] Dellaert F (2005) Square root SAM: Simultaneous localization and mapping via square root information smoothing. In: Robotics: Science and Systems
[10] Dellaert F, Kaess M (2006) Square root SAM: Simultaneous localization and mapping via square root information smoothing. International Journal of Robotics Research
[11] Durrant-Whyte H, Bailey T (2006) Simultaneous localisation and mapping (SLAM): Part I the essential algorithms. Robotics and Automation Magazine
[12] Folkesson J, Christensen H (2004) Graphical SLAM - a self-correcting map. International Conference on Robotics and Automation
[13] Folkesson J, Jensfelt P, Christensen H (2007) The M-Space feature representation for SLAM. IEEE Transactions on Robotics 23(5):1024–1035
[14] Jason M, LaValle S (2007) Localization with limited sensing. IEEE Transations on Robotics 23:704–716
[15] Kaess M, Ranganathan A, Dellaert F (2007) Fast incremental square root information smoothing. In: Internation Joint Conference on Artificial Intelligence
[16] Kaess M, Ranganathan A, Dellaert F (2008) iSAM: Incremental smoothing and mapping. IEEE Transactions on Robotics (Forthcoming)
[17] Müller M, Surmann H, Pervölz K, May S (2006) The accuracy of 6D SLAM using the AIS 3D laser scanner. In: International Conference on Multisensor Fusion and Integration for Intelligent Systems
[18] Nguyen V, Martinelli A, Tomatis N, Siegwart R (2005) A comparison of line extraction algorithms using 2D laser rangefinder for indoor mobile robotics. In: IEEE International Conference on Intelligent Robots and Systems, pp 1929–1934
[19] O'Kane J, LaValle S (2005) Almost-sensorless localization. In: IEEE International Conference on Robotics and Automation, pp 3764–3769
[20] Smith R, Cheeseman P (1987) On the representation and estimation of spatial uncertainty. International Journal of Robotics Research 5(4):56–68